A Method for Calculating the Optimal Velocity Search Step Size for Airborne Three-Channel SAR Adaptive Clutter Suppression

Yongkang Li , Yingcong Wang , Yonghui Zhang , Baochang Liu ,
and Hongmeng Chen , *Senior Member, IEEE*

Abstract—For multichannel synthetic aperture radar (SAR) ground moving target indication (GMTI) systems, the clutter suppression method based on post-Doppler space time adaptive processing technology is popular due to its excellent performance. However, to coherently integrate a target's energy of each channel, this kind of method requires a search of target's velocity, which would introduce a large computation load when the search step size is too small. While the existing studies mainly focus on improving its performance in the cases of complex scenes and geometries, the studies on optimizing the search step size are rare. To address this issue, this article proposes a method for calculating the optimal velocity search step size of adaptive clutter suppression for the commonly used airborne three-channel SAR-GMTI systems. First, the signal models in the range Doppler domain are developed. Then, considering that both the signal-to-clutter-noise ratio loss of clutter suppression and the coherent integration gain loss are introduced by the mismatch of target's steer vector, the relationship between the coherent accumulation gain loss and the velocity search error is utilized to develop the analytical expression for the optimal velocity search step size. Experimental results validate the proposed method.

Index Terms—Clutter suppression, ground moving target indication (GMTI), synthetic aperture radar (SAR).

I. INTRODUCTION

SYNTHETIC aperture radar (SAR) is a microwave imaging radar that is known for its high resolution, all-weather, and all-day capabilities. It has found widespread applications in fields, such as agriculture monitoring, ocean observation, and military reconnaissance [1], [2], [3]. Ground moving target

Yongkang Li is with the School of Electronics and Information, Northwestern Polytechnical University, Xi'an 710072, China, and also with the Research & Development Institute of Northwestern Polytechnical University in Shenzhen, Shenzhen 518063, China (e-mail: yongkang_li@foxmail.com).

Yingcong Wang and Yonghui Zhang are with the School of Electronics and Information, Northwestern Polytechnical University, Xi'an 710072, China.

Baochang Liu is with the School of Marine Sciences, Nanjing University of Information Science and Technology, Nanjing 210044, China.

Hongmeng Chen is with the Beijing Institute of Radio Measurement, Beijing 100854, China.

indication (GMTI) is an important operational mode of SAR. SAR-GMTI systems are capable of indicating moving targets within the illustrated scene while simultaneously providing high-resolution image of the stationary scene. They have played a significant role in military reconnaissance, traffic monitoring, etc. [4], [5], [6], [7].

Clutter suppression is a crucial way to improve the performance of multichannel SAR-GMTI systems. It effectively enhances the signal-to-clutter-noise ratio (SCNR), and thus can facilitate the increase of target detection probability and parameter estimation accuracy. In the field of multichannel SAR-GMTI, clutter suppression methods could be generally divided into two main categories: methods based on displaced phase center antenna technology and methods based on space-time adaptive processing (STAP) technology [8]. The latter have gained significant attentions in recent years due to its stronger clutter suppression capability and the ability to coherently accumulate target signals across multiple channels.

Due to the long coherent integration time of SAR, the clutter data of various Doppler cells are statistically independent [9]. Therefore, the post-Doppler STAP technique can be utilized to suppress the clutter adaptively for multichannel SAR. Many relevant studies have been presented in recent years [9], [10], [11], [12], [13]. For instance, Cerutti-Maori et al. [9] presented a detailed analysis of the signal characteristics of target and clutter in the range-Doppler domain, and combined post-Doppler STAP with SAR imaging to propose the imaging STAP (ISTAP) method. Silva et al. [10] investigated the use of prior road information to enhance the clutter suppression performance under heterogeneous scenes. In addition, Chang et al. [11] extended the ISTAP method to geosynchronous-orbit SAR.

In order to accumulate the energy of target signals from various channels coherently, adaptive clutter suppression based on post-Doppler STAP requires the construction of accurate steering vector using target's motion parameters. However, in practice, moving targets are noncooperative, and their motion parameters are unknown. Therefore, the adaptive clutter suppression requires a search of target's motion parameters, and a small search step size may result in a heavy computational burden, while a large search step size may lead to a significant loss of SCNR. Nevertheless, existing researches are mainly focused on improving the performance of the adaptive clutter suppression in cases of heterogeneous scenes, complex observation geometries,
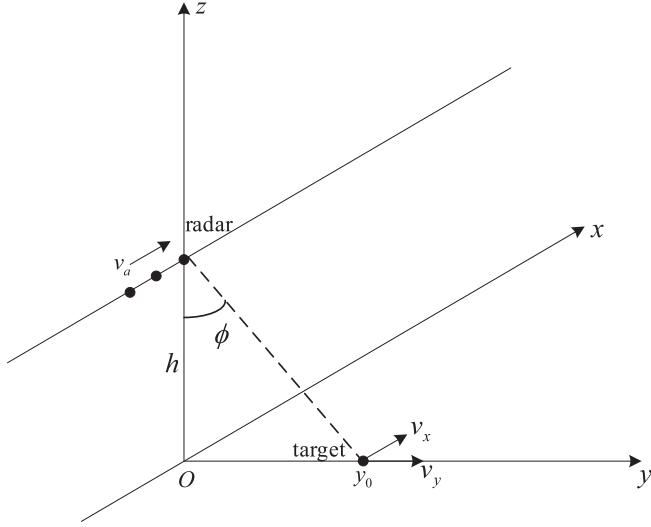
Fig. 1. Geometry of an airborne three-channel SAR-GMTI system.

and so on [10], [11], [12], [13]. The studies on optimizing the search step size are rare.

To achieve a good balance between the computational efficiency and clutter suppression performance, this article studies the determination of the optimal velocity search step size for adaptive clutter suppression with the allowable SCNR loss being 3 dB. In this article, the signal models in the range-Doppler domain for the commonly used airborne three-channel SAR-GMTI system are established. Moreover, considering that both the output SCNR loss of clutter suppression and the coherent accumulation gain loss of target are caused by the mismatch of steering vector, the relationship between the coherent accumulation gain loss and the velocity search error is utilized to develop the analytical expression for calculating the optimal velocity search step size.

The rest of this article is organized as follows. In Section II, the signal models in the range Doppler domain are established. Section III briefly introduces the principle of adaptive clutter suppression based on post-Doppler STAP technology. In Section IV, the proposed method for determining the optimal search step size of target's velocity is introduced. Section V presents experimental results to validate the effectiveness of the proposed method. Finally, Section VI concludes this article.

II. SIGNAL MODELING

The geometry of an airborne three-channel SAR is shown in Fig. 1. The height and velocity of the radar platform are h and v_a, respectively. The distance between adjacent effective phase centers of the radar is d. At the azimuth slow time $t_a = 0$, the effective phase center of the channel 1 is located in $(0,0,h)$, and that of nth ($n = 2,3$) channel is located in $(-(n-1)d,0,h)$. Assume that there exists a moving target on the ground at $(0,y_0,0)$, whose velocities along the x- and y-axes are v_x and v_y, respectively.

According to Fig. 1, the instantaneous slant range between the moving target and the effective phase center of nth ($n = 1,2,3$) channel can be expressed as

$$R_n(t_a) = \sqrt{[v_x t_a - v_a t_a + (n-1)d]^2 + (y_0 + v_y t_a)^2 + h^2}. \quad (1)$$

Applying a second-order Taylor expansion to the above equation around $t_a = 0$, one can obtain

$$R_n(t_a) \approx R_0 + \left[\frac{(v_x - v_a)(n-1)d}{R_0} + v_y \sin\phi\right] t_a$$
$$+ \frac{(v_x - v_a)^2 + v_y^2(1 - \sin^2\phi)}{2R_0} t_a^2 \quad (2)$$

where $R_0 = \sqrt{h^2 + y_0^2}$ represents the distance from the target to the radar at $t_a = 0$, and ϕ denotes the radar's look-down angle.

After carrier frequency demodulation and range compression, the received echo signal in the raw data domain for nth channel can be represented as

$$s_n(t_r, t_a) = p_r\left(t_r - \frac{2R_n(t_a)}{c}\right) w_{a,n}(t_a)$$
$$\exp\left\{-j4\pi\frac{R_n(t_a)}{\lambda}\right\} \quad (3)$$

where $p_r(\cdot)$ is the range-compressed pulse response, $w_{a,n}(\cdot)$ is the azimuth envelope, c is the speed of light, λ is the wavelength, and t_r is range fast time.

After channel calibration and coregistration [14] with channel 1 as the reference channel, the signal for nth channel can be represented as [4]

$$s_{n,\text{reg}}(t_r, t_a) = p_r\left(t_r - \frac{2R_{n,\text{reg}}(t_a)}{c}\right) w_{a,1}(t_a)$$
$$\exp\left\{-j4\pi\frac{R_{n,\text{reg}}(t_a)}{\lambda}\right\} \quad (4)$$

with

$$R_{n,\text{reg}}(t_a) = R_n\left(t_a + \frac{(n-1)d}{v_a}\right)$$
$$\approx R_1(t_a) + v_y \sin\phi\frac{(n-1)d}{v_a} \quad (5)$$

where $R_{n,\text{reg}}(t_a)$ represents the target range equation for channel n after coregistration. The detailed derivation for (5) is provided in Appendix A.

Applying an azimuthal Fourier transform to (4) and using the principle of stationary phase, the signal in the range-Doppler domain can be expressed as

$$S_{n,\text{reg}}(t_r, f_a)$$
$$\approx p_r\left\{t_r - \frac{2}{c}\left[R_0 - \frac{\lambda}{4}\left(\frac{f_a^2 - \frac{4v_y^2\sin^2\phi}{\lambda}}{\frac{4(v_x - v_a)^4 + 4v_y^4(1 - \sin^2\phi)^4}{\lambda^2 R_0^2}}\right)\right]\right\}$$
$$\times W_a\left(f_a + \frac{2v_y\sin\phi}{\lambda}\right)$$
$$\cdot \exp\left\{-j\frac{4\pi}{\lambda}\left(R_0 + \frac{v_y^2(1 - \sin^2\phi)}{2R_0}\right)\right\}$$
$$\times \exp$$
$$\left\{j\frac{\pi\lambda R_0}{2(v_x - v_a)^2 + 2v_y^2(1 - \sin^2\phi)^2}\left(f_a + \frac{2v_y\sin\phi}{\lambda}\right)^2\right\}$$

$$\times \exp \left\{ -j \frac{4\pi v_y \sin \phi \,(n-1)\, d}{\lambda}\frac{(n-1)\, d}{v_a} \right\} \tag{6}$$

where f_a represents the azimuth frequency, and $W_a\,(\cdot)$ is the azimuth frequency envelope.

According to the equation above, the target steering vector in the range-Doppler domain can be expressed as

$$s_t = \left[1, \quad e^{-j \frac{4\pi v_y \sin \phi}{\lambda} \cdot \frac{d}{v_a}}, \quad \dots \quad e^{-j(N-1)\frac{4\pi v_y \sin \phi}{\lambda} \cdot \frac{d}{v_a}} \right]^T$$

$$= \left[1, \quad e^{j\varphi}, \quad \dots \quad e^{(N-1)\varphi} \right]^T \tag{7}$$

where $\varphi = -\frac{4\pi v_y \sin \phi}{\lambda} \cdot \frac{d}{v_a}$. As can be seen from (7), the steering vector is depended on v_y.

By setting the velocities in (6) and (7) to be zeros, i.e., $v_x = 0$, $v_y = 0$, we can obtain the clutter signal $C_{n,\,\mathrm{reg}}\,(t_r, f_a)$ and its steering vector s_c as follows:

$$C_{n,\mathrm{reg}}\,(t_r, f_a) \approx p_r \left[t_r - \frac{2}{c}\left(R_0 - \frac{\lambda^3 R_0{}^2 f_a^2}{16 v_a{}^4} \right) \right] W_a\,(f_a)$$

$$\times \exp\left\{ -j\frac{4\pi}{\lambda} R_0 \right\} \exp\left\{ j \frac{\pi \lambda R_0}{2 v_a{}^2} f_a{}^2 \right\} \tag{8}$$

$$s_c = [1, 1, \dots, 1]^T. \tag{9}$$

III. ADAPTIVE CLUTTER SUPPRESSION BASED ON POST-DOPPLER STAP

The optimal weight vector based on post-Doppler STAP can be represented as [9]

$$W_{\mathrm{opt}} = \frac{R^{-1} s_t}{s_t{}^H R^{-1} s_t} \tag{10}$$

where R represents the covariance matrix of clutter and noise, which can be expressed as

$$R = E\left[Z_{cn} Z_{cn}{}^H \right]$$

$$= R_c + R_n \tag{11}$$

where Z_{cn} represents the clutter and noise signal, R_c is the clutter covariance matrix, and R_n is the noise covariance matrix.

The output signal of adaptive clutter suppression is

$$T = W_{\mathrm{opt}}{}^H Z \tag{12}$$

where Z represents the echo signal in the range-Doppler domain received by the radar.

The above adaptive clutter suppression can obtain a significant SCNR improvement, because, on the one hand, it can suppress clutter well, on the other hand, it can coherently accumulate the target signals of each channel. However, it can be seen from (10) that the target's velocity is needed when constructing the optimal weight. This will result in a search of target's velocity during the clutter suppression, because the motion parameters of the target are usually unknown in practice. Obviously, using a smaller search step size will result in a better SCNR improvement, but a larger computational burden. Therefore, it is necessary to study the method for determining the optimal search step size, so as to achieve a good balance between the computational efficiency and clutter suppression performance.

IV. METHOD FOR DETERMINING THE OPTIMAL SEARCH STEP SIZE

This section will develop a method for determining the optimal search step size of target's velocity with the allowable SCNR loss being 3 dB.

Assuming that the target's velocity along the y-axis used for a certain search is $v_y + \Delta v_y$ then the steering vector used for constructing the weight vector can be represented as follows:

$$q =$$
$$\left[1, \quad e^{-j\frac{4\pi(v_y + \Delta v_y)\sin\phi}{\lambda} \cdot \frac{d}{v_a}}, \quad \dots \quad e^{-j(N-1)\frac{4\pi(v_y + \Delta v_y)\sin\phi}{\lambda}\frac{d}{v_a}} \right]^T$$

$$= \left[1, \quad e^{j\varphi_\Delta}, \quad \dots \quad e^{(N-1)\varphi_\Delta} \right]^T \tag{13}$$

where $\varphi_\Delta = -\frac{4\pi(v_y + \Delta v_y)\sin\phi}{\lambda} \cdot \frac{d}{v_a}$.

When the above steering vector is not mismatched, i.e., $q = s_t$, the constructed weight vector is the optimal weight vector shown in (10). In this case, the optimal output SCNR can be expressed as follows:

$$\mathrm{SCNR}_{\mathrm{opt}} = \frac{\sigma_s{}^2 \left| W_{\mathrm{opt}}{}^H s_t \right|^2}{W_{\mathrm{opt}}{}^H R W_{\mathrm{opt}}}$$

$$= \sigma_s{}^2 \cdot s_t{}^H R^{-1} s_t \tag{14}$$

where $\sigma_s{}^2$ represents the signal power. The detailed derivation for (14) is presented in Appendix B.

When the steering vector is mismatched, i.e., $q \neq s_t$, the constructed weight vector is

$$W_{\mathrm{mis}} = \frac{R^{-1} q}{q^H R^{-1} q}. \tag{15}$$

In this case, the output SCNR can be expressed as

$$\mathrm{SCNR}_{\mathrm{mis}} = \frac{\sigma_s^2 \left| W_{\mathrm{mis}}{}^H \cdot s_t \right|^2}{W_{\mathrm{mis}}{}^H R W_{\mathrm{mis}}}. \tag{16}$$

After several common mathematical operations, (16) can be rewritten as

$$\mathrm{SCNR}_{\mathrm{mis}} = \mathrm{SCNR}_{\mathrm{opt}} \cdot \frac{\left| q^H R^{-1} s_t \right|^2}{\left(s_t{}^H R^{-1} s_t \right)\left(q^H R^{-1} q \right)}. \tag{17}$$

The detailed derivations for (16) and (17) are provided in Appendix B.

From (17), it can be seen that the SCNR loss due to the mismatch of the steering vector can be expressed as

$$L_{\mathrm{scnr}} = \frac{\left| q^H R^{-1} s_t \right|^2}{\left(s_t{}^H R^{-1} s_t \right)\left(q^H R^{-1} q \right)}. \tag{18}$$

The above SCNR loss is related to the velocity error Δv_y. However, (18) is quite complex, and it is very difficult to derive an analytical expression for the relationship between the SCNR loss and Δv_y. Since the SCNR loss is mainly caused by the accumulation loss of target energy across multiple channels, the following coherent accumulation gain loss is utilized instead:

$$L_{\mathrm{cag}} = \frac{\left| q^H \cdot s_t \right|}{s_t{}^H \cdot s_t}. \tag{19}$$

TABLE I
SYSTEM PARAMETERS OF REAL DATA

Parameter	Value
Platform velocity	106.7 m/s
Carrier frequency	9.6 GHz
Effective phase center separation	0.172 m
PRF	833.3 Hz
Slant range of scene center	32.68 km
Synthetic aperture time	2.46 s
CNR	44.18 dB
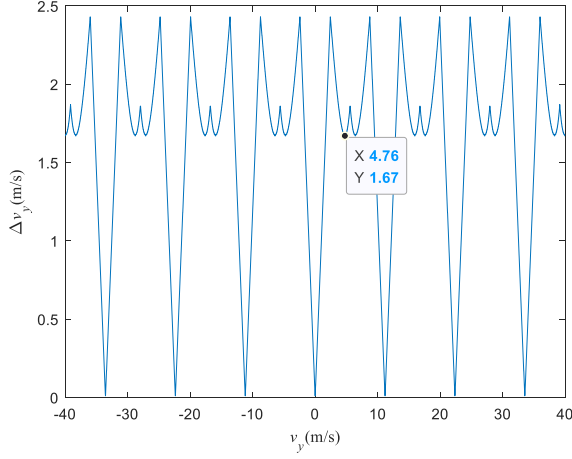
Fig. 2.   Velocity search errors for a SCNR loss of 3 dB under different v_y.
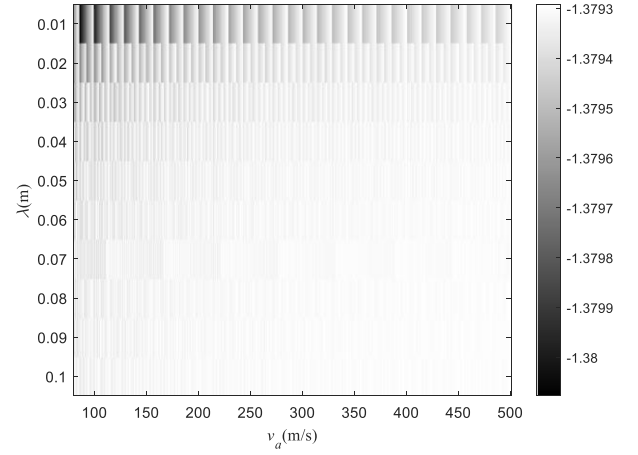

Fig. 3.   Values of $L_{\text{cag}}(\Delta v_{y,\min})$ for different pairs of λ and v_a with $d = 0.2$ m (the color represents the value and the unit is in dB).
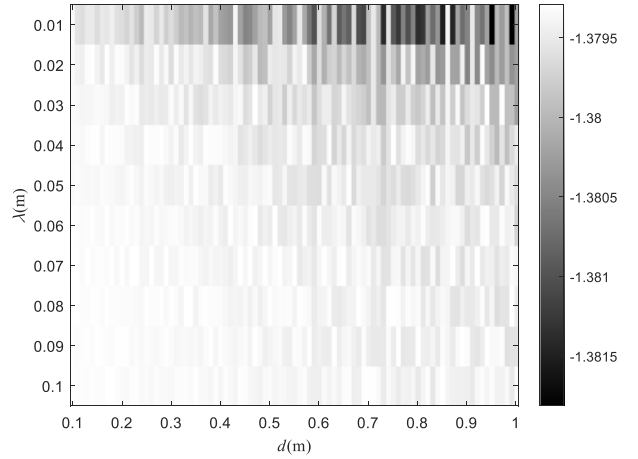

Fig. 4.   Values of $L_{\text{cag}}(\Delta v_{y,\min})$ for different pairs of λ and d with $v_a = 120$ m (the color represents the value and the unit is in dB).

Substituting (7) and (13) into (19), and simplifying via the sine double-angle formula, we can obtain

$$
\begin{aligned}
L_{\text{cag}} &= \frac{1}{3} \frac{\sin\left(\frac{3}{2} \cdot (\varphi - \varphi_\Delta)\right)}{\sin\left(\frac{1}{2} \cdot (\varphi - \varphi_\Delta)\right)} \\
&= 1 - \frac{4}{3}\sin^2\left[\frac{1}{2} \cdot (\varphi - \varphi_\Delta)\right] \\
&= 1 - \frac{4}{3}\left(\frac{1 - \cos(\varphi - \varphi_\Delta)}{2}\right) \\
&= \frac{1}{3} + \frac{2}{3}\cos(\varphi - \varphi_\Delta) \\
&= \frac{1}{3} + \frac{2}{3}\cos\left(\frac{4\pi \Delta v_y \sin\phi}{\lambda} \frac{d}{v_a}\right).
\end{aligned}
\tag{20}
$$

With (20), the analytical expression for L_{cag} in terms of velocity error is obtained. Since L_{scnr} and L_{cag} are both determined by the difference between φ and φ_Δ, there is a one-to-one correspondence between them. In the following, numerical analysis is adopted to obtain the relationship between L_{scnr} and L_{cag}, and then the analytic expression for calculating the optimal velocity search step size will be obtained.

In order to derive the relationship between the SCNR loss and velocity error, the value of L_{cag} when $L_{\text{scnr}} = -3$ dB is investigated via numerical simulations. The parameters used in the simulation are given in Table I. First, through ergodic search, the velocity search error Δv_y that makes L_{scnr} be -3 dB for different v_y is found out, as shown in Fig. 2.

As can be seen from Fig. 2, Δv_y varies periodical with v_y, and there are seven blind speeds in the interval $[-40$ m/s, 40 m/s]. Without considering the blind speeds and their adjacent velocities, from Fig. 2 it can be find out that the minimum value of Δv_y is 1.67 m/s. Therefore, as long as the velocity search error is less than 1.67 m/s, the SCNR loss will be less than 3 dB. In other words, for this system, when the allowable SCNR loss is 3 dB, the optimal (minimum) velocity search error $\Delta v_{y,\min}$ is 1.67 m/s.

By substituting the above optimal value of the velocity error into (20), it can be figured out that $L_{\text{cag}}(\Delta v_{y,\min})$ is -1.38 dB. Moreover, through numerical simulation, the following interesting phenomenon is found out: even if the radar system parameters are changed (including the wavelength, baseline length, and radar velocity), $L_{\text{cag}}(\Delta v_{y,\min})$ is approximated to be -1.38 dB, where $\Delta v_{y,\min}$ is the minimum velocity search error for an allowable SCNR loss of 3 dB. The values of $L_{\text{cag}}(\Delta v_{y,\min})$ for different system parameters are shown in Figs. 3– 5. Note that the value of $\Delta v_{y,\min}$ varies with the system parameters.

Therefore, based on (20), by letting $L_{\text{cag}}(\Delta v_{y,\min})$ be -1.38 dB, the analytic expression for $\Delta v_{y,\min}$ can be figured
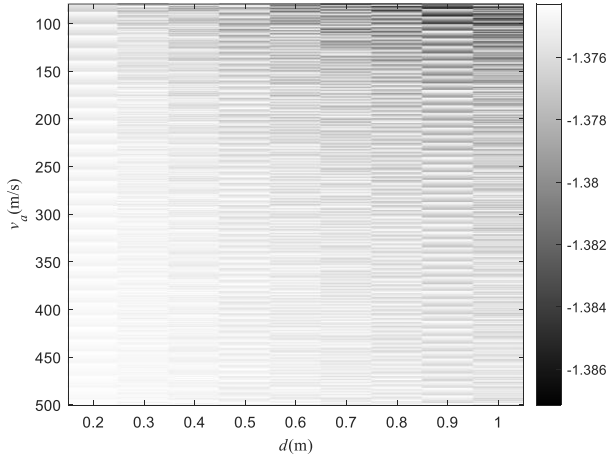
Fig. 5. Values of $L_{\text{cag}}(\Delta v_{y,\min})$ for different pairs of d and v_a with $\lambda = 0.03$ m (the color represents the value and the unit is in dB).

Fig. 6. Clutter data in the range Doppler domain.

TABLE II
TARGET MOTION PARAMETERS

Target	v_x	v_y
T1	10.23 m/s	−18.29 m/s
T2	−5.14 m/s	−14.93 m/s
T3	5.14 m/s	−4.93 m/s
T4	6.37 m/s	28.47 m/s
T5	−10.47 m/s	38.49 m/s

out

$$\Delta v_{y,\min} = \frac{\lambda k v_a}{4\pi d \sin \phi} \qquad (21)$$

with $k = \arccos(\frac{3}{2} \times 10^{-0.138} - \frac{1}{2})$.

Since the velocity search error does not exceed half of the velocity search step size, the optimal velocity search step size $\Delta v_{y,\text{opt}}$ is twice the optimal search error. Thus, the analytic expression for the optimal velocity search step size is as follows:

$$\Delta v_{y,\text{opt}} = \frac{\lambda k v_a}{2\pi d \sin \phi}. \qquad (22)$$

Therefore, when the system parameters of the radar are known, the optimal search step size can be figured out via (22).

V. EXPERIMENTAL RESULTS

In this section, experiments are carried out to verify the effectiveness of the proposed method for determining the optimal search step size. For the experiments, the background clutter is real data of an X-band three-channel airborne SAR-GMTI system, whose system parameters are given in Table I. Fig. 6 shows the real clutter data in the range Doppler domain after range compression.

A. Results of Simulated Targets

Five moving targets are simulated. Their velocity parameters are given in Table II, and they are assumed to be located in the center of the scene. The signal-to-clutter ratio is set to −10 dB.
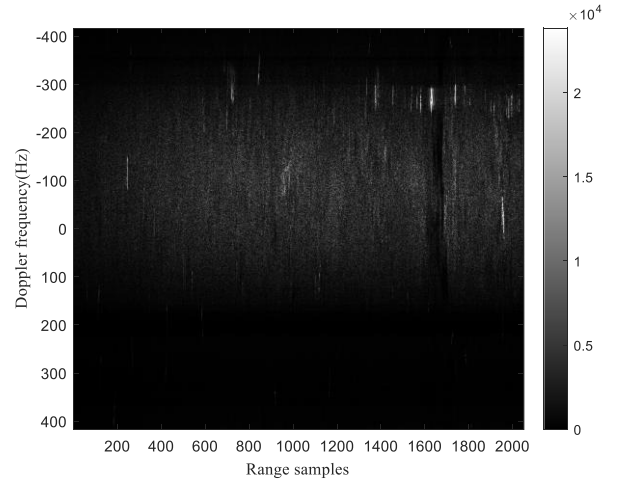
Note that the motion parameters of the five targets are carefully set so that the search error is close to half of the search step size. In addition, the optimal search step size calculated according to (22) is 3.34 m/s. The covariance matrix for clutter suppression is estimated from the real data, and the coherence between the calibrated data of different channels is 0.98.

Taking target T2 as an example, the data before clutter suppression in the range Doppler domain is shown in Fig. 7(a). It can be seen that the target is overwhelmed by clutter. Fig. 7(b) shows the result of adaptive clutter suppression using the target's real velocity, and the measured SCNR in this case is 16.19 dB. Fig. 7(c) shows the results of adaptive clutter suppression based on the optimal search step size, and the measured SCNR in this case is 13.64 dB. As can be seen from Fig. 7, after clutter suppression, the clutter energy is significantly suppressed, and the target can be clearly distinguished. In addition, it can be seen that the energy of the target signal in Fig. 7(c) is less than that of the target in Fig. 7(b) because of the velocity search error.

The SCNR loss of each target by clutter suppression using the optimal search step size is measured and presented in Table III. It can be seen that the SCNR losses are all within 3 dB.

B. Results of Comparative Experiments With Different Velocity Search Step Sizes

In order to illustrate the superiority of the proposed method in balancing the computational efficiency and clutter suppression performance, comparative experiments using two different velocity search step sizes are carried out with the targets simulated in Section V-A.

The two search steps used are 0.6 times the optimal step size and 1.5 times the optimal step size. The measured SCNR losses are presented in Tables IV and V, respectively. The measured runtimes of these three search step sizes are given in Table VI.

From Tables III–VI it can be seen that, overall, the smallest search step size has the best clutter suppression performance, but it also has the longest runtime. In addition, as can be seen from Table V, for the 1.5 times the optimal step size, the SCNR losses of T4 and T5 are larger than 3 dB. The very small loss of
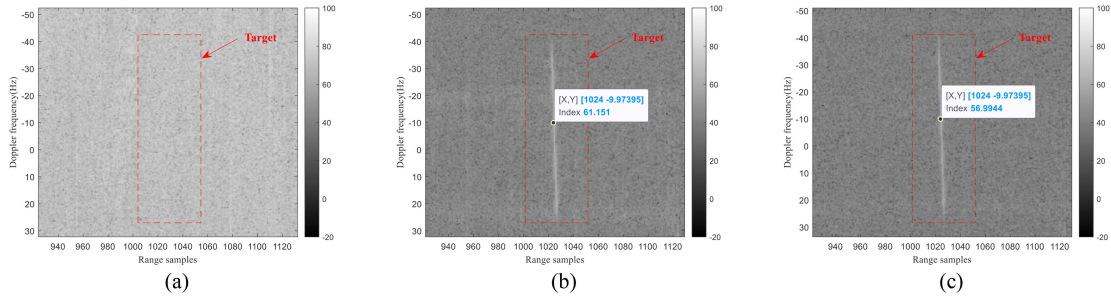
Fig. 7.   Experimental results of target T2. (a) Range Doppler domain data before clutter suppression. (b) Clutter suppression results using the real velocity. (c) Clutter suppression results using the optimal search step size.

TABLE III
SCNR LOSSES USING THE OPTIMAL SEARCH STEP SIZE

Target	Output SCNR for clutter suppression with target's real velocity	Output SCNR for clutter suppression using the optimal search step size	SCNR loss
T1	16.98 dB	15.10 dB	1.88 dB
T2	16.19 dB	13.64 dB	2.55 dB
T3	16.42 dB	13.82 dB	2.60 dB
T4	16.44 dB	13.72 dB	2.72 dB
T5	16.86 dB	14.49 dB	2.37 dB

TABLE IV
SCNR LOSSES USING 0.6 TIMES THE OPTIMAL SEARCH STEP SIZE

Target	Output SCNR for clutter suppression using 0.6 times the optimal search step size	SCNR loss
T1	15.85 dB	1.13 dB
T2	15.79 dB	0.40 dB
T3	15.94 dB	0.48 dB
T4	16.39 dB	0.05 dB
T5	16.05 dB	0.81 dB

TABLE V
SCNR LOSSES USING 1.5 TIMES THE OPTIMAL SEARCH STEP SIZE

Target	Output SCNR for clutter suppression using 1.5 times the optimal search step size	SCNR loss
T1	15.27 dB	1.71 dB
T2	16.16 dB	0.03 dB
T3	16.42 dB	0.00 dB
T4	13.23 dB	3.21 dB
T5	9.27 dB	7.59 dB

TABLE VI
RUNTIMES OF THE USED SEARCH STEPS

Search step	Runtime
0.6 times the optimal search step size	46.54 s
The optimal search step size	27.57 s
1.5 times the optimal search step size	18.77 s

TABLE VII
MOTION PARAMETERS OF THE MULTIPLE TARGETS

Target	v_x	v_y
T6	−15.78 m/s	−16.29 m/s
T7	23.57 m/s	−15.45 m/s
T8	7.94 m/s	−14.91 m/s

achieve a moderate runtime while ensuring the SCNR losses being within 3 dB.

C. Results of Real Target

There are real moving targets in the background clutter data. However, they are noncooperative targets, and their motion parameters are unknown. To further validate the proposed method, a real moving target is found out. We first roughly estimate its radial velocity, and the result is 11.2 m/s. Then, via a refined search around the estimated value, we obtain a more accurate estimation of the velocity, and the result is 11.36 m/s.

The clutter suppression results are given in Fig. 8, and the measured output SCNR for clutter suppression using the accurately estimated velocity and the optimal search step size are 30.90 and 30.04 dB, respectively. From Fig. 8(b) and (c), one can see that the clutter is effectively suppressed and the target can be clearly distinguished. Moreover, it can be figured out that the SCNR loss relative to the accurately estimated velocity is 0.86 dB, which is within 3 dB.

D. Results of Multiple Moving Targets

In practice, there may be multiple moving targets. For the cases where the radial velocities of these targets are close, these targets can be simultaneously processed by the proposed

SCNR for T2 and T3 is due to the fact that the searched velocities happen to be very close to their true velocities. Moreover, from Tables III and VI one can see that the optimal step size can

TABLE VIII
SCNR LOSSES OF MULTIPLE MOVING TARGETS

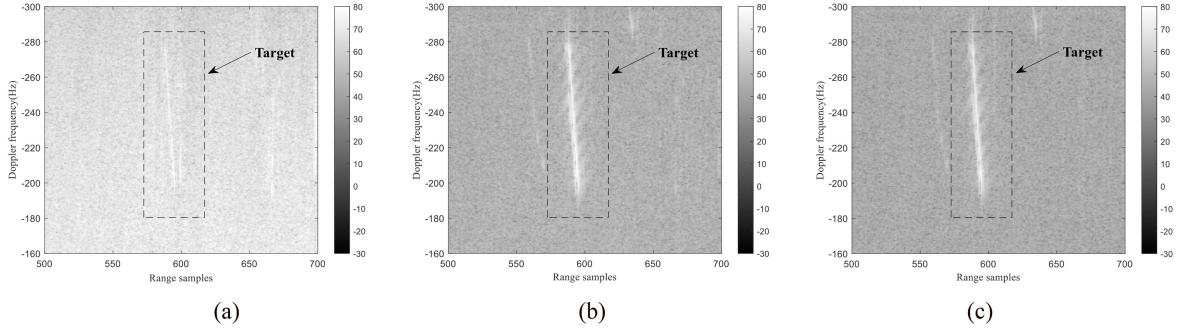| Target	Output SCNR for clutter suppression with target's real velocity	Output SCNR for clutter suppression using the optimal search step size	SCNR loss
T6	13.11 dB	12.89 dB	0.22 dB
T7	17.06 dB	16.06 dB	1.00 dB
T8	15.35 dB	12.59 dB	2.76 dB

Fig. 8.　Experimental results of the real target. (a) Range Doppler domain data before clutter suppression. (b) Clutter suppression results using the accurately estimated velocity. (c) Clutter suppression results using the optimal search step size.
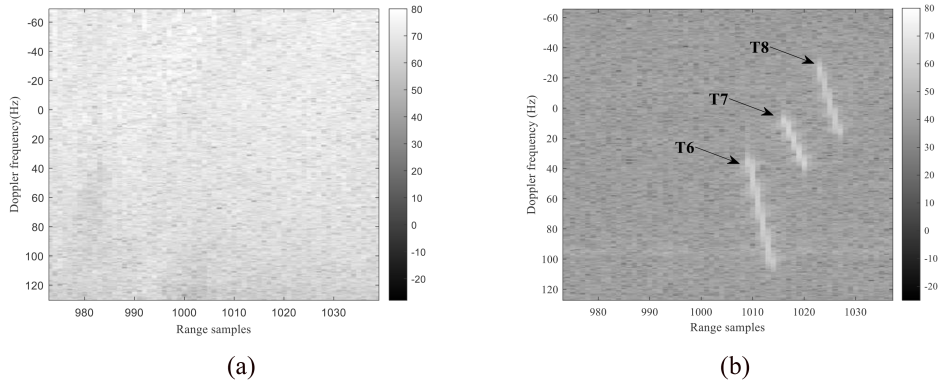

Fig. 9.　Results of clutter suppression for multiple moving targets. (a) Before clutter suppression. (b) After clutter suppression.

method. Note that there is no restriction on the targets' along-track velocities.

To validate above statement, three moving targets are simulated, and their parameters are presented in Table VII. The experimental results are shown in Fig. 9 and Table VIII, and the velocity used in clutter suppression is -16.62 m/s. From these results it can be seen that the clutter is effectively suppressed and the SCNR losses are all within 3 dB.

VI. CONCLUSION

In this article, we have proposed a method to determine the optimal velocity search step size for airborne three-channel SAR adaptive clutter suppression, so as to achieve a good balance between the computational efficiency and clutter suppression performance. The analytical expression for calculating the optimal step size of velocity search with an allowable SCNR loss of 3 dB has been developed. Experimental results have verified the effectiveness of the proposed method.

For the cases where the allowable SCNR losses are not 3 dB, the method presented in Section III may also be utilized to obtain the analytical expression for the optimal velocity search step size. For instance, our studies show that, when the allowable SCNR losses are 2 and 1 dB, the optimal search step size can also be calculated by (22) with k being $\arccos(1.5 \times 10^{-0.091} - 0.5)$ and $\arccos(1.5 \times 10^{-0.0045} - 0.5)$, respectively.

For the cases where the number of channels is larger than 3, since the sine double-angle formula cannot be used to simplify (20), it is very difficult to obtain a concise analytic expression for the optimal step size like (22).

APPENDIX A

The derivation of (5) is presented in this appendix.

According to (2), $R_n(t_a + (n-1)d/v_a)$ can be expressed as (23) shown at the bottom of the next page.

Equation (23) can be further expressed as (24) shown at the bottom of the next page, with (25) shown at the bottom of the next page.

Since the maximum value of $\Delta(t_a)$ is significant less than $\lambda/16$, it can be neglected [15]. Thus, $R_{n,\mathrm{reg}}(t_a)$ can be expressed as

$$R_{n,\mathrm{reg}}(t_a) = R_n\left(t_a + \frac{(n-1)d}{v_a}\right)$$

$$\approx R_1(t_a) + v_y \sin\phi \frac{(n-1)d}{v_a}. \tag{26}$$

The correctness of (26) is verified by numerical experiments as follows. The system parameters used in the simulations are the same as those in Table I. Fig. 10 shows the relationship between the maximum value of the error $\Delta(t_a)$ and target's motion parameters, with the color indicating the magnitude in meters. As can be seen from Fig. 10, for all possible target motion parameters, the maximum value of $\Delta(t_a)$ is significant less than $\lambda/16$ (1.96×10^{-3} m), and thus it can be ignored [15].

APPENDIX B

The derivations of (14), (16), and (17) are presented in this appendix.

According to (9) and (11), $\boldsymbol{R}_c$ and $\boldsymbol{R}_n$ are Hermitian matrices. Therefore, $\boldsymbol{R}$ is a Hermitian matrix and the following equation holds:

$$\left(\boldsymbol{R}^{-1}\right)^H = \boldsymbol{R}^{-1}. \tag{27}$$
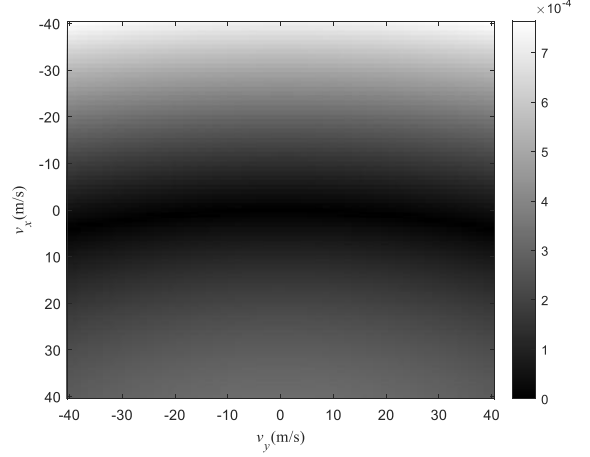

Fig. 10. Relationship between the maximum value of the error $\Delta(t_a)$ and target's motion parameters.

Thus, (14) can be simplified as follows:

$$\mathrm{SCNR}_{\mathrm{opt}} = \frac{\sigma_s^2 \left|\boldsymbol{W}_{\mathrm{opt}}^H \boldsymbol{s}_t\right|^2}{\boldsymbol{W}_{\mathrm{opt}}^H \boldsymbol{R} \boldsymbol{W}_{\mathrm{opt}}}$$

$$= \frac{\sigma_s^2 \left|\frac{\boldsymbol{s}_t^H \boldsymbol{R}^{-1}}{\boldsymbol{s}_t^H \boldsymbol{R}^{-1} \boldsymbol{s}_t} \boldsymbol{s}_t\right|^2}{\frac{\boldsymbol{s}_t^H \boldsymbol{R}^{-1}}{\boldsymbol{s}_t^H \boldsymbol{R}^{-1} \boldsymbol{s}_t} \boldsymbol{R} \frac{\boldsymbol{R}^{-1} \boldsymbol{s}_t}{\boldsymbol{s}_t^H \boldsymbol{R}^{-1} \boldsymbol{s}_t}}$$

$$= \sigma_s^2 \cdot \boldsymbol{s}_t^H \boldsymbol{R}^{-1} \boldsymbol{s}_t. \tag{28}$$

$$R_n\left(t_a + \frac{(n-1)d}{v_a}\right) = R_0 + \left[\frac{(v_x - v_a)(n-1)d}{R_0} + v_y \sin\phi\right]\left(t_a + \frac{(n-1)d}{v_a}\right) + \frac{(v_x - v_a)^2 + v_y^2\left(1 - \sin^2\phi\right)}{2R_0}$$

$$\left(t_a + \frac{(n-1)d}{v_a}\right)^2 = R_0 + \left[\frac{(v_x - v_a)(n-1)d}{R_0} + v_y \sin\phi\right]t_a + \left[\frac{(v_x - v_a)(n-1)d}{R_0} + v_y \sin\phi\right]\frac{(n-1)d}{v_a}$$

$$+ \frac{(v_x - v_a)^2 + v_y^2\left(1 - \sin^2\phi\right)}{2R_0}t_a^2 + \frac{(v_x - v_a)^2 + v_y^2\left(1 - \sin^2\phi\right)}{R_0}\frac{(n-1)d}{v_a}t_a$$

$$+ \frac{(v_x - v_a)^2 + v_y^2\left(1 - \sin^2\phi\right)}{2R_0}\frac{(n-1)^2 d^2}{v_a^2}. \tag{23}$$

$$R_n\left(t_a + \frac{(n-1)d}{v_a}\right) = R_1(t_a) + \frac{(v_x - v_a)(n-1)d}{R_0}t_a + v_y \sin\phi \frac{(n-1)d}{v_a} + \frac{(v_x - v_a)(n-1)^2 d^2}{v_a R_0}$$

$$+ \frac{(v_x - v_a)^2 + v_y^2\left(1 - \sin^2\phi\right)}{R_0}\frac{(n-1)d}{v_a}t_a + \frac{(v_x - v_a)^2 + v_y^2\left(1 - \sin^2\phi\right)}{2R_0}\frac{(n-1)^2 d^2}{v_a^2}$$

$$= R_1(t_a) + v_y \sin\phi \frac{(n-1)d}{v_a} + \Delta(t_a) \tag{24}$$

$$\Delta(t_a) = \frac{(v_x - v_a)(n-1)d}{R_0}t_a + \frac{(v_x - v_a)(n-1)^2 d^2}{v_a R_0}$$

$$+ \frac{(v_x - v_a)^2 + v_y^2\left(1 - \sin^2\phi\right)}{R_0}\frac{(n-1)d}{v_a}t_a + \frac{(v_x - v_a)^2 + v_y^2\left(1 - \sin^2\phi\right)}{2R_0}\frac{(n-1)^2 d^2}{v_a^2}. \tag{25}$$

Similarly, (16) and (17) can be simplified as follows:

$$
\begin{aligned}
\text{SCNR}_{\text{mis}} &= \frac{\sigma_s^2 \left| \boldsymbol{W}_{\text{mis}}{}^H \cdot \boldsymbol{s}_t \right|^2}{\boldsymbol{W}_{\text{mis}}{}^H \boldsymbol{R} \boldsymbol{W}_{\text{mis}}} \\
&= \sigma_s^2 \frac{\left| \boldsymbol{q}^H \boldsymbol{R}^{-1} \boldsymbol{s}_t \right|^2}{\boldsymbol{q}^H \boldsymbol{R}^{-1} \boldsymbol{q}} \\
&= \sigma_s^2 \cdot \boldsymbol{s}_t{}^H \boldsymbol{R}^{-1} \boldsymbol{s}_t \frac{\left| \boldsymbol{q}^H \boldsymbol{R}^{-1} \boldsymbol{s}_t \right|^2}{\left(\boldsymbol{q}^H \boldsymbol{R}^{-1} \boldsymbol{q} \right) \left(\boldsymbol{s}_t{}^H \boldsymbol{R}^{-1} \boldsymbol{s} \right)} \\
&= \text{SCNR}_{\text{opt}} \cdot \frac{\left| \boldsymbol{q}^H \boldsymbol{R}^{-1} \boldsymbol{s}_t \right|^2}{\left(\boldsymbol{q}^H \boldsymbol{R}^{-1} \boldsymbol{q} \right) \left(\boldsymbol{s}_t{}^H \boldsymbol{R}^{-1} \boldsymbol{s} \right)}. \quad (29)
\end{aligned}
$$

REFERENCES

[1] I. G. Cumming and F. H. Wong, *Digital Processing of Synthetic Aperture Radar Data Algorithm and Implementation*. Norwood, MA, USA: Artech House, 2005.

[2] Y. Zhang, D. Zhu, X. Mao, X. Yu, J. Zhang, and Y. Li, "Multirotors video synthetic aperture radar: System development and signal processing," *IEEE Aerosp. Electron. Syst. Mag.*, vol. 35, no. 12, pp. 32–43, Dec. 2020.

[3] G. Xu, B. Zhang, H. Yu, J. Chen, M. Xing, and W. Hong, "Sparse synthetic aperture radar imaging from compressed sensing and machine learning: Theories, applications, and trends," *IEEE Geosci. Remote Sens. Mag.*, vol. 10, no. 4, pp. 32–69, Dec. 2022.

[4] S. V. Baumgartner and G. Krieger, "Multi-channel SAR for ground moving target indication," *Academic Press Library Signal Process.*, vol. 2, pp. 911–986, Feb. 2014.

[5] X. Zhang, G. Liao, S. Zhu, C. Zeng, and Y. Shu, "Geometry-information-aided efficient radial velocity estimation for moving target imaging and location based on radon transform," *IEEE Trans. Geosci. Remote Sens.*, vol. 53, no. 2, pp. 1105–1117, Feb. 2015.

[6] P. Lombardo, D. Pastina, and F. Turin, "Ground moving target detection based on MIMO SAR systems," *IEEE J. Sel. Topics Appl. Earth Observ. Remote Sens.*, vol. 8, no. 11, pp. 5081–5095, Nov. 2015.

[7] B. Ge, D. An, L. Chen, W. Wang, D. Feng, and Z. Zhou, "Ground moving target detection and trajectory reconstruction methods for multichannel airborne circular SAR," *IEEE Trans. Aerosp. Electron. Syst.*, vol. 58, no. 4, pp. 2900–2915, Aug. 2022.

[8] J. H. G. Ender, C. H. Gierull, and D. Cerutti-Maori, "Improved space-based moving target indication via alternate transmission and receiver switching," *IEEE Trans. Geosci. Remote Sens.*, vol. 46, no. 12, pp. 3960–3974, Dec. 2008.

[9] D. Cerutti-Maori, I. Sikaneta, and C. H. Gierull, "Optimum SAR/GMTI processing and its application to the radar satellite RADARSAT-2 for traffic monitoring," *IEEE Trans. Geosci. Remote Sens.*, vol. 50, no. 10, pp. 3868–3881, Oct. 2012.

[10] A. B. C. da Silva, S. V. Baumgartner, and G. Krieger, "Training data selection and update strategies for airborne post-Doppler STAP," *IEEE Trans. Geosci. Remote Sens.*, vol. 57, no. 8, pp. 5626–5641, Aug. 2019.

[11] C. Chang, X. Dong, Z. Chen, C. Hu, and W. Tian, "A long-time coherent integration STAP for GEO spaceborne-airborne bistatic SAR," *Remote Sens.*, vol. 14, no. 3, 2022, Art. no. 593.

[12] X. Li, Z. Yang, S. He, P. Huang, G. Liao, and Y. Jiang, "Nonhomogeneous clutter suppression based on terrain elevation interferometric phase compensation in multi-satellite formation systems," *Digit. Signal Process.*, vol. 121, Mar. 2022, Art. no. 103282.

[13] Z. Li et al., "Bistatic SAR clutter-ridge matched STAP method for nonstationary clutter suppression," *IEEE Trans. Geosci. Remote Sens.*, vol. 60, Feb. 2022, Art. no. 5216914.

[14] J. Ender et al., "The airborne experimental multi-channel SAR-system AER-II," in *Synthetic Aperture Radar: EUSAR'96*, Berlin, Germany: Springer-Verlag, 1996, pp. 49–52.

[15] G. C. Walter, S. G. Ron, and M. M. Ronald, *Spotlight Synthetic Aperture Radar, Signal Processing Algorithms*. Norwood, MA, USA: Artech House, 1995.

Yongkang Li was born in Hunan, China. He received the B.Eng. degree in electronic information engineering and the Ph.D. degree in signal and information processing from Xidian University, Xi'an, China, in 2011 and 2016, respectively.

From 2015 to 2016, he was a Visiting Researcher with the School of Electrical and Electronic Engineering, Nanyang Technological University, Singapore. Since 2022, he has been an Associate Professor with the School of Electronics and Information, Northwestern Polytechnical University, Xi'an. His research interests include SAR-GMTI, SAR imaging, and clutter suppression.

Yingcong Wang was born in Hunan, China. He received the B.S. degree in communications engineering in 2021 from Northwestern Polytechnical University, Xi'an, China, where he is currently working toward the M.S. degree in information and communication engineering with the School of Electronic Information.

His research interests include SAR-GMTI and clutter suppression.

Yonghui Zhang was born in Henan, China. He received the B.S. degree in electronic information engineering from Hohai University, Nanjing, China, in 2022. He is currently working toward the M.S. degree in electronic information with the School of Electronic Information, Northwestern Polytechnical University, Xi'an, China.

His research interests include MEO SAR-GMTI and curved trajectory SAR imaging.
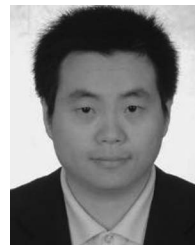
Baochang Liu was born in Shandong, China. He received the B.S. degree in electrical engineering from Liaocheng University, Liaocheng, China, in 2004, and the Ph.D. degree in signal and information processing from the National Laboratory of Radar Signal Processing, Xidian University, Xi'an, China, in 2010.

He is currently an Associate Professor with the School of Marine Sciences, Nanjing University of Information Science and Technology, Nanjing, China. He has authored or coauthored more than 20 research articles in the area of his research interests which include multichannel/multidimensional synthetic aperture radar (SAR) system design and signal processing, high-resolution wide-swath SAR, moving target indication, and ocean microwave remote sensing.

Hongmeng Chen (Senior Member, IEEE) received the B.S. degree in communication engineering from Nanchang University, Nanchang, China, in 2008, and the M.S. and Ph.D. degrees in information and communication engineering from the National Laboratory of Radar Signal Processing, Xidian University, Xi'an, China, in 2012 and 2016, respectively.

From 2016 to 2019, he was a Postdoctoral Researcher with the Second Academy of China Aerospace Science and Industry Corporation, Beijing, China. He is currently a Senior Engineer with the Beijing Institute of Radio Measurement, Beijing. His research interests include synthetic aperture radar (SAR)/inverse SAR (ISAR) imaging, forward-looking radar imaging, ground moving target indication (GMTI), and motion parameter estimation.